Current Journal of Applied Science and Technology

Volume 43, Issue 1, Page 17-34, 2024; Article no.CJAST.111497
ISSN: 2457-1024
(Past name: British Journal of Applied Science & Technology, Past ISSN: 2231-0843, NLM ID: 101664541)

Predictive Modeling and Analysis of Thermal Failure in Plastic and Composite Gears Using VDI Method Approach

Y. N. Agbetossou [a*], K. F. Wotodzo [a], D. Koffi [b], L. Nyametso [a], K. A. Kassegne [a++] and S. Tiem [a++]

[a] Laboratory of Structures and Mechanics of Materials (LaS2M) - Department of Mechanical Engineering, Polytechnic School of Lomé, University of Lomé, 01 B.P. 1515 Lomé 1, Togo.
[b] Institute of Innovation in Ecomaterials, Ecoproducts and Ecoenergy (I2E3) of the University of Quebec at Trois-Rivières, CP 500, Trois-Rivières, Quebec, G9A 5H7, Canada.

Authors' contributions

This work was carried out in collaboration among all authors. All authors read and approved the final manuscript.

Article Information

DOI: 10.9734/CJAST/2024/v43i14340

Open Peer Review History:
This journal follows the Advanced Open Peer Review policy. Identity of the Reviewers, Editor(s) and additional Reviewers, peer review comments, different versions of the manuscript, comments of the editors, etc are available here: https://www.sdiarticle5.com/review-history/111497

Original Research Article

Received: 11/11/2023
Accepted: 15/01/2024
Published: 20/01/2024

ABSTRACT

A method for predicting surface thermal failure of gears made of plastic materials and their natural fiber composites is developed with the "Verein Deutscher Ingenieure (VDI)" "Association of German Engineers" method, and a simulation is made for these gears.
The simulation is carried out for Duracon acetal gears and composite material of high density polyethylene (HDPE) with 40% birch wood fiber (HDPE40B) gears. The simulation is carried out with the same meshing characteristics that were used to carry out the tests on the gear test bench in real simulated operation to study the thermo-tribo-mechanical behavior of HDPE40B gears.

[++]Professor;
**Corresponding author: E-mail: niconay@yahoo.fr;*

From the predefined operating temperature, the torque-speed (C-ω) limiting curve is established using the computer program for predicting operating temperatures. Then the heat map is established using the same temperature calculation program by determining the equilibrium temperatures in the tooth and instantaneous temperatures on the profile according to the normalized positions S/pn. The induced surface contact stresses are then determined according to the normalized positions S/pn with the VDI method and are compared with the limit allowable stress.
The results show that more severe operating conditions give comparatively lower induced stresses, but they are nevertheless the ones that will fail first at surface thermal failure compared to less severe operating conditions. In other words, the results show that the more severe the operating conditions, the shorter the operating cycles become before surface thermal failure occurs.
The results also show that the surface thermal failure behaviors for plastics and composites gears are similar and the higher the melting temperature of the material, the butter it can stand surface thermal failure in more severe working conditions.

Keywords: Plastic and composite gears; thermal failure prediction; C-ω limiting curve; simulation; MATLAB.

LIST OF SYMBOLS AND ABBREVIATIONS

VDI : Verein Deutscher Ingenieure (Association of German Engineers);
HDPE : High density polyethylene;
HDPE40B : Composite of high density polyethylene with 40% in weight of birch wood fiber;
C-ω : Torque-speed;
PV : Pressure and Velocity product;
T_{fo} *: Operating limit temperature;*
T_f *: Melting temperature of the material;*
H : coeficient, 0<η<1;
TB_1, TB_2 *: Equilibrium temperatures of teeth for driver and driven gears;*
TF_1, TF_2 *: Instantaneous temperatures on teeth profile for driver and driven gears;*
σ_{oc} *: Contact stress;*
F_t *: Tangential bending force;*
$SIGMA_C$ *: Induced contact stress following the normalized positions on the tooth profile;*
$SIGMA_CLM55$ *: Allowable fatigue stress under operating condition of (C=5.5Nm, ω=500 rpm, Number of cycle 10^6);*
$SIGMA_CLM7$ *: Allowable fatigue stress under operating condition of (C=7Nm, ω=1500 rpm, Number of cycle 10^6);*
$SIGMA_CLM86885$ *: Allowable fatigue stress under operating condition of (C=8.6885Nm, ω=1000 rpm, Number of cycle 10^6);*
$SIGMA_C55$ *: Induced stress under operating condition of (C=5.5Nm, ω=500 rpm);*
$SIGMA_C7$ *: Induced stress under operating condition of (C=7Nm, ω=1500 rpm);*
$SIGMA_C86885$ *: Induced stress under operating condition of (C=8.6885Nm, ω=1000 rpm);*

1. INTRODUCTION

The use of plastic materials in the manufacture of gears found in motion and even power transmission mechanisms is increasing [1-3]. This is due to the low cost of these materials and that of appropriate implementation, such as injection molding, combined with their exclusive intrinsic properties, including shock and vibration absorption, minimizing weight and durability, inertia, the reduction and integration of lubrication in the material, or without lubrication, among others, and above all the possibility of integrating the gear and other parts in a single injection molded element, in complex shapes, defying any metalworking technique [9,13]. So today, the best gear for a given application is often made of plastic [3] and both suppliers (Shell, DuPont, Celanese, etc.) and machine manufacturers compete in ingenuity to show applications in various fields, office automation, household appliances, automobile industry [4,5].

However, the pronounced variation in the mechanical properties of these materials with temperature poses a problem for their use in the field of gears. A particular mode of failure called "thermal" is added to those already encountered

in metal gears, such as failure by bending fatigue at the root of the tooth, that of contact on the surface of the tooth and wear excessive. Thermal failure manifests itself in two forms [1]:

- Surface thermal failure: due to localized softening of the tooth profile under the effect of excessive temperature leading to melting of the material, tearing of material and deterioration of the profile;

- Generalized thermal failure: due to the softening of the entire tooth following the loss of the mechanical properties of the material under the effect of hysteresis and friction heat; it results in bending under load (creep type) leading to permanent deformation, inadequate functional clearances or catastrophic failure. The tooth can sometimes melt completely, or break at the root (very rare for plastics) or in the vicinity of the pitch point.

The work of various researchers reported in the literature has shown that wear combined with heating still remains the main cause of failure to plastic gears and their composites [12,13].

Much work has been carried out on the two classical modes of bending at the root and the Hertz stress at the surface for both metallic and plastic gears [1]. Similarly, studies have been carried out on the wear of profiles in metal gears [8]. There is also numerous experimental work on the wear of plastic-to-metal mesh [8]. Likewise, apart from the few experimental works on profile wear in plastic-on-plastic gears which existed before 2015, notably the work of Mao et al. [6] and that of Kukureka et al. [8], the experimental work have multiplied in recent years for the wear of the profile of gear teeth made of plastic materials, bio-plastics and their eco-composites, such as the work of Wafiuddin et al. [16], of Singh et al. [17] and Herba et al. [18]. For surface and generalized thermal failure, they have not been the subject of specific studies to date [1], nevertheless the work of Koffi et al. [7] laid the basis for their verifications.

In this present work, the study of the prediction of surface thermal failure is addressed. First, a method for predicting surface thermal failure is studied. Then the characteristic data of the materials studied and the meshing conditions are presented. After that, the different stages of the simulation are exposed, then followed by the presentation of the results. Finally, the work is concluded.

2. STUDY OF A METHOD FOR MODELING AND PREDICTING SURFACE THERMAL FAILURE

As said previously, surface and generalized thermal failure are modes of damage specific to plastic gears and their composites. To study their modeling and prediction, Koffi et al. [7] carried out a preliminary analysis and recommended the various essential points to take into account. For surface thermal Failure, these points are as follows:

- The creation of the thermal map in steady state for the equilibrium temperature of the tooth and in transient mode for the instantaneous surface temperature on the contact profile;
- Calculation of the distribution of the induced contact stress over the entire contact profile;
- Comparison of the induced contact stress with the allowable stress;
- The calculation of the stress and the meshing speed on the contact profile, and the comparison of these quantities to the PV limits of the materials.

Based on these recommendations, we propose a comprehensive seven-point method.

Step1- Define the operating limit temperature (T_{fo}) for the application such as:

$$T_{f0} = \eta T_f \qquad (1)$$

With $0<\eta<1$. T_f is the melting temperature of the material.

Step2- Choose a temperature prediction model for plastic gears and their composites; (analytical or numerical: i. e. Block; Hackman and Strikle; D. Koffi, etc...)

Step3- Establish the C-ω (PV) limiting curve, using the operating limit temperature T_{fo}. The C-ω limiting curve (load C in Nm and rotation speed ω in rpm), replaces the limit curve (PV) of the material for a specific application. It is established using the temperature prediction program, such that any point (C, ω) of the curve, generates instantaneous temperatures TF_1 and TF_2 verifying the condition $\max(TF_1,TF_2)=T_{fo}$.

Step4- Establish the heat map by determining the distribution of the equilibrium temperature in the tooth and the instantaneous temperatures on the active profile of the tooth. The equilibrium temperature heat map shows the distribution in the tooth of the average temperature reached by the tooth during its operation. The thermal map of the instantaneous temperature shows the evolution of the instantaneous temperature of the tooth profile according to the normalized positions S/pn on the action line and its variation inside the contact zone.

Step5- Calculation of the contact stress distribution over the entire profile with the VDI2545 method using instantaneous temperatures to determine the Young's modulus as a function of temperature;

$$\sigma_{oc} = \sqrt{\frac{F_t}{bd}\frac{u+1}{u}(K_A)}Z_H Z_M Z_\varepsilon \leq \frac{\sigma_{HN}}{S_{H\min}} \quad (2)$$

K_A: application factor; Z_H: form factor; Z_M: material factor; Zε: contact ratio factor.

Step6- Compare the induced contact stress and the allowable stress;

Step7- Check that each operating point following the normalized positions S/pn is below the C-ω limiting curve; otherwise no operating temperature should be higher than T_{fo}. This point is in reality guaranteed by the condition of establishing the curve C-ω.

3. CHARACTERISTIC DATA FOR THE SIMULATION OF SURFACE THERMAL FAILURE

We do the simulation with our new composite material HDPE40B and the acetal material Duracon M90 commonly used in the field of plastic gears (Tables 1 and 2). Tables 1 to 4 and fig. 1 to 7 present the tables and characteristic curves of the HDPE40B materials and Duracon M90 acetal which were used for the thermal failure study.

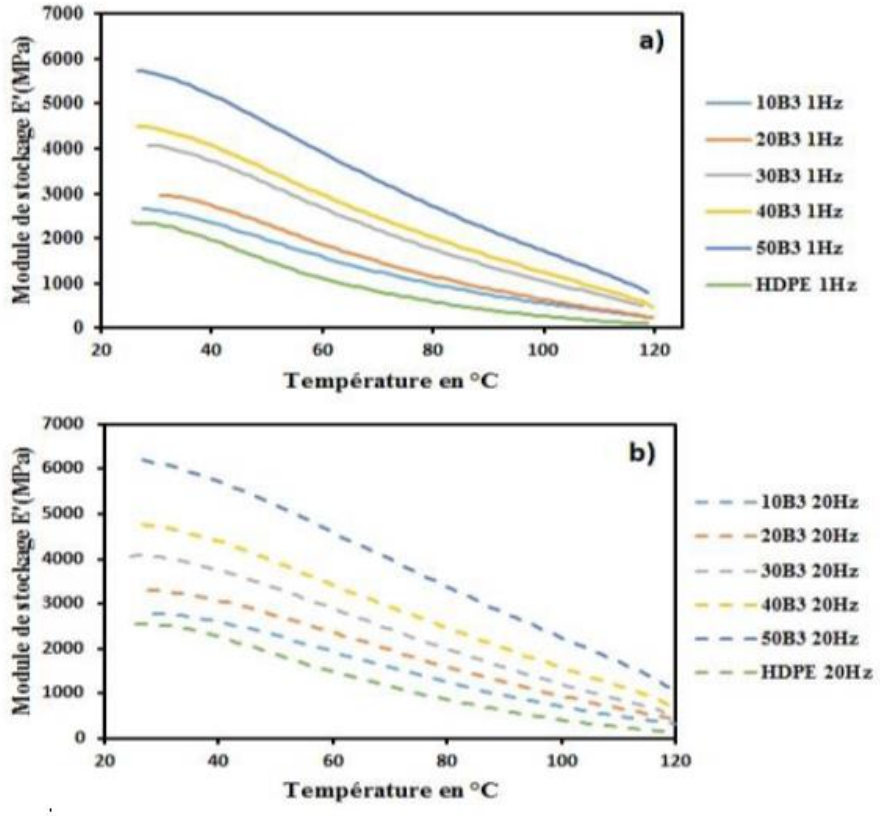

Fig. 1. Storage modulus E' with different wood fiber (birch) rates for frequencies a) 1Hz and b) 20Hz as a function of temperature [11]

Table 1. Material characteristics [11, 14]

Parameters	Materials			
	UHMWPE	**Nylon**	**Acetal Duracon M90**	**HDPE40B**
Specific weight: ρ (kg/m^3)	941.12	1140	1410	1185.6
Young modulus: E (GPa)	0.68	2.85	2.88	3.45
Poisson coefficient: $\boldsymbol{\upsilon}$	0.41	0.4	0.35	0.33
Thermal conductibility: k (w/m.K)	0.6747	0.250	0.228	0.7870
Specific heat : C (J/kg.K)	2301.2	2750	1470	1325.104
Friction coefficient: μ	0.5	0.28	0.21	0.20
Melting temperature : T_f (°C)	130	215	165	140

Table 2. Specifications for the thermal failure simulation

HDPE40B	**Acetal Duracon M90**
Module : m=2.54mm or diametral pitch D_P=10	Module : m=2mm or diametral pitch D_P=12.7
Number of teeth : Z_1= Z_2=30	Number of teeth : Z_1= Z_2=30
Pressure angle : α =20°	Pressure angle : α =20°
Tooth width : b=6.5mm	Tooth width : b=6.5mm
Rotation speed : $\boldsymbol{\omega}_1$, $\boldsymbol{\omega}_2$= 0 - 2500 rpm	Rotation speed : $\boldsymbol{\omega}_1$, $\boldsymbol{\omega}_2$= 0 - 2500 rpm
Torque : T = 0 - 12.5 Nm	Torque : T = 0 - 9.7 Nm

Table 3. Determination of the allowable tangential bending force at the pitch circle and the allowable bending fatigue stress for Duracon M90 acetal [14]

Duracon M90

The allowable tangential force F (kgf) at pitch circle of a Duracon M90 spur gear can also be obtained from the Lewis formula.

$$F = my\sigma_b \ (kgf) \quad (3)$$

Where:
m = Module (mm)
y = Form factor at pitch point
b = Teeth width (mm)
σ_b = Allowable bending stress (kgf/mm^2)

The allowable bending stress can be calculated by **Equation** (4)

$$\sigma_b = \sigma_b' \frac{K_V K_T K_L K_M}{C_S} \quad (4)$$

Where:

σ_b' = Maximum allowable bending stress under ideal condition (see Fig. 2)
C_S = Working factor (see table 4)
K_V = Speed factor (see Fig. 3)
K_T = Temperature factor (see Fig. 4)
K_L = Lubrication factor (see Table 4)
K_M = Material factor (see Table 4)

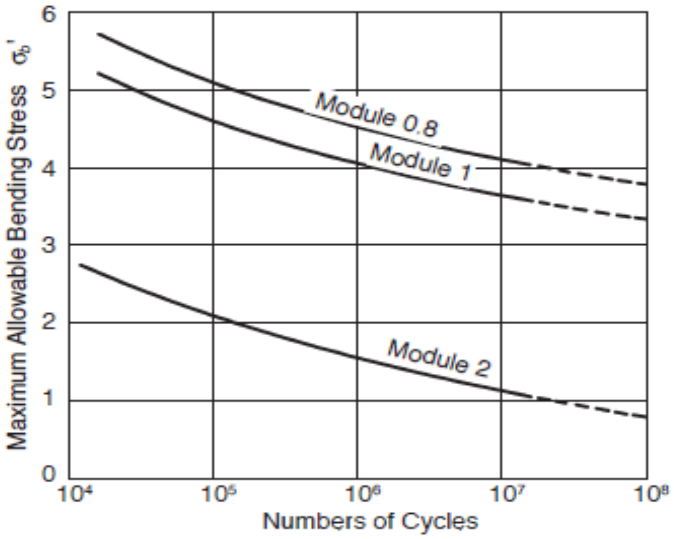

Fig. 2. Maximum allowable bending fatigue stress under ideal conditions for acetal M90 [14]

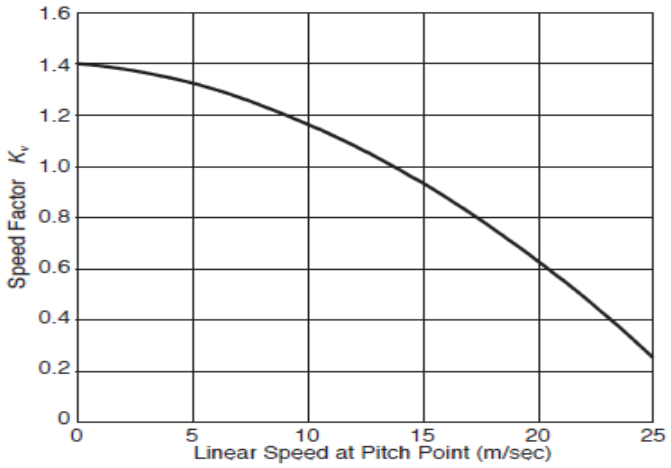

Fig. 3- Speed factor Kv for acetal M90 [14]

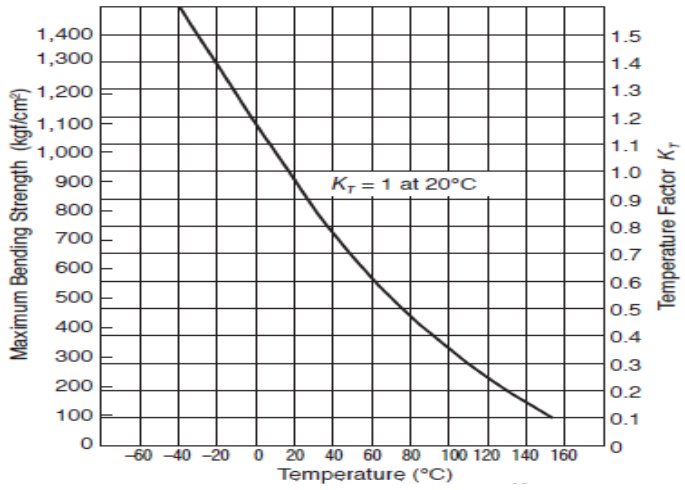

Fig. 4. Temperature factor K_T for acetal M90 [14]

Table 4. Working condition factor, lubrication factor and material factor for determining the allowable stress of bending fatigue [14]

Type of Load	Working Factor C_S			
	Daily Operating Hours			
	24 hrs/day	8 – 10 hrs/day	0.5 hrs/day	3 hrs/day
Uniform Load	1.25	1.00	0.80	0.50
Light impact	1.50	1.25	1.00	0.80
Medium impact	1.75	1.50	1.25	1.00
Heavy impact	2.00	1.75	1.25	1.25
Lubrication factor K_L				
Initial grease lubrication			1	
Continuous Oil lubrication			1.5 - 3	
Material Factor K_M				
Material Combination			K_M	
Duracon vs Metal			1	
Duracon vs Duracon			0.75	

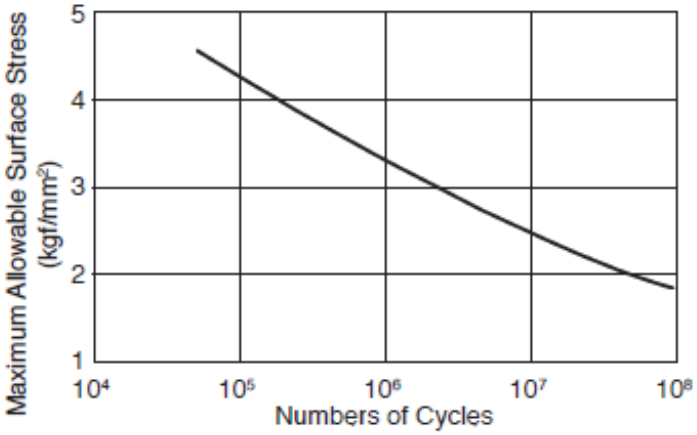

Fig. 5. Maximum allowable contact fatigue stress under the conditions specify here below for acetal M90 [14]

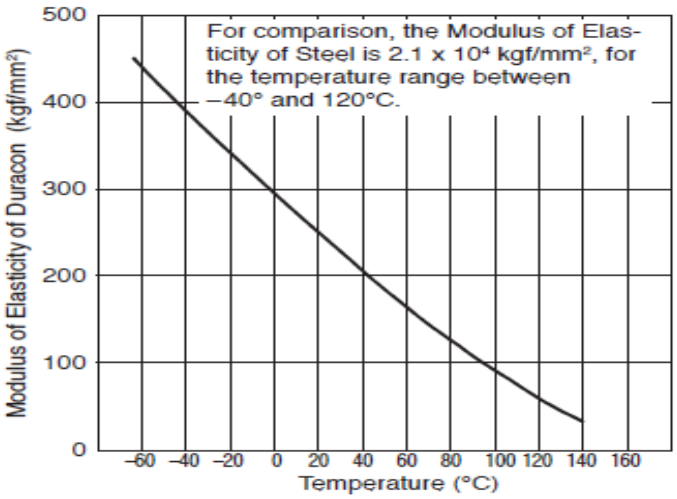

Fig. 6. Elasticity modulus as function of temperature for acetal M90 [14]

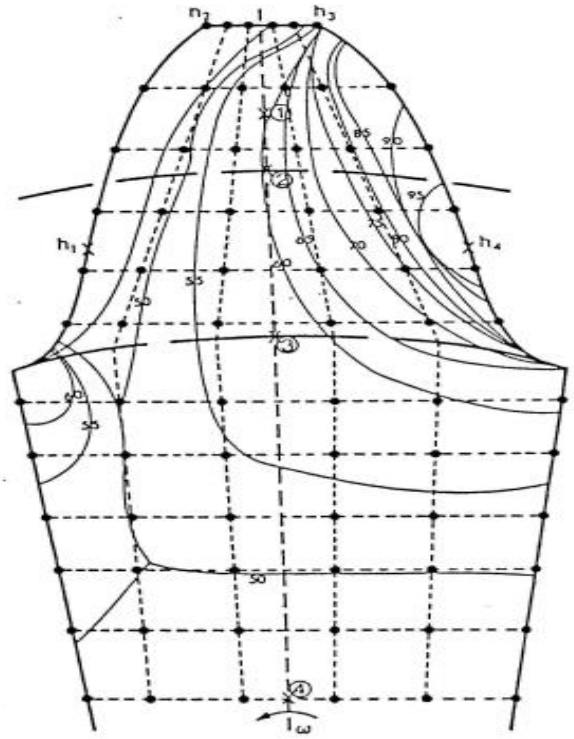

Fig. 7. Tooth geometry mesh [10]

Fig. 5- is based upon data for a pair of Duracon gears: m = 2, v = 12 m/s, and operating at room temperature. For working conditions that are similar or better, the values in the Fig. can be used [14]

4. THERMAL FAILURE SIMULATION METHODOLOGY

The complete simulation stages are as follow:

- **Definition of operating temperatures**

For our two study cases, we estimate that the operating temperature can rise up to 80% of the melting temperature, i.e. η=0.8. So for the case of the HDPE40B material, $T_{fo}=0.8T_f=140°Cx0.8=112°C$ and for the case of the Duracon M90 material, $T_{fo}=0.8T_f=165°Cx0.8=132°C$.

- **Choice of the temperature prediction model and establishment of the C-ω limiting curve**

The numerical model of Koffi et al. [10] is chosen and the initial FORTRAN program is translated into MATLAB. For the HDPE40B material, we establish the C-ω limiting curve such that for all positions S/pn, the (P, V), or the (C, ω) give a maximum instantaneous temperature TF_1max or TF_2max which is approximately T_{fo} =112°C. By varying ω between 0 rpm and 2500 rpm we obtain, using our MATLAB temperature prediction program, the following points (ω, C): (0, 12.5); (500, 12.5); (907, 12.5); (1000, 11.5); (1500, 8.1745); (2000, 6.4); (2500, 5.3385) for the C-ω limiting curve. The curve obtained is presented in the results. Thus, for any operating point (ω, C) below the C-ω limits curve, the operating temperature is below T_{fo}. For the acetal material Duracon M90, $T_{fo}=0.8T_f=165°Cx0.8=132°C$, we establish the C-ω limiting curve such that for all positions S/pn, the (P, V), or the (C, ω) give a maximum instantaneous temperature TF_1max or TF_2max which is approximately T_{fo} =132°C. By varying ω between 0 rpm and 2500 rpm we obtain, using our MATLAB temperature prediction program, the following points (ω, C): (0, 9.769); (500, 9.769); (863.9.769); (1000, 8.6885); (1500, 6.265); (2000, 4.9092); (2500, 4.0369) for the C-ω limiting curve.

- **Establishing the heat map**

Using the temperature prediction program, we established the thermal maps of the driving gear and the driven gear.

- **Calculation of the contact stress distribution over the entire profile**

The contact stress on the tooth profile is calculated based on the normalized position S/pn by the formula of VDI 2545.

$$\sigma_{oc} = \sqrt{\frac{F_t}{bd}\frac{u+1}{u}(K_A)}Z_H Z_M Z_\varepsilon \leq \frac{\sigma_{HN}}{S_{H\min}} \quad (5)$$

With:

F_t the tangential load;
The force F_t can be calculated by:

$$F_t(S/pn) = \frac{C}{R}\frac{W_i}{W_n} = \frac{2PC}{Z}\frac{W_i}{W_n} \quad (6)$$

where C is the torque applied to the axis of the driving gear, R is the radius of the pitch circle, d is the pitch diameter, Z is the number of teeth and P is the diametral pitch.
For the plastic / plastic mesh case which interests us more particularly in this study, we have:

$$\frac{W_i}{W_n}\left(\frac{s}{P_n}\right) = \left.\frac{W_i}{W_n}\right|_0 \cos\left(\frac{\pi}{2}\frac{s/P_n}{s_2''/P_n}\right) \quad (7)$$

With:

$$\left.\frac{W_i}{W_n}\right|_0 = 0.48.E_2^{-0.28}\left(W_0.P\cos\alpha\right)^{-0.22}Z_2^{-0.4}\left(\frac{Z_2}{Z_1}\right)^{0.1} \quad (8)$$

Where $\left.\frac{W_i}{W_n}\right|_0$ is the value of the load distribution factor at the pitch point (s = 0).
Wn is the total load along the line of action transmitted to all the teeth in contact.
Wi is the load transmitted along the line of action to the main tooth meshing in position Si.

$$Wo = Wn/b = (2PC/Z\cos\alpha)/b. \quad (9)$$

b is the tooth width.

K_A the application factor which is fixed in agreement between the manufacturer and the user; in the absence of agreement, we set K_A = 1. In this calculation we set K_A = 1
Z_H the flank form factor is calculated for the spur gears as follows;

$$Z_H = \frac{1}{\cos\alpha_t}\sqrt{\frac{\cos\beta_b}{tg\alpha_{t\omega}}} \quad (10)$$

α_t = pressure angle at the reference pitch circle;
$\alpha_{t\omega}$ = operating pressure angle apparent to the original reference circle;
β_b = basic helix angle;

$$\cos\beta_b = \cos\beta\frac{\cos\alpha_n}{\cos\alpha_t} \quad (11)$$

Information is provided for teeth without offset (α = 20 °), Z_H = 1.7 and 1.6 for teeth with offset. For our calculations we will take Z_H = 1.7 because we are in the presence of teeth without offset with the pressure angle α = 20 °.
Zε driving factor; for spur gear teeth we have:

$$Z_\varepsilon = \sqrt{\frac{4-\varepsilon_\alpha}{3}} \quad (12)$$

For our simulation it remains to determine the modules E_1 and E_2 as a function of the temperatures TF_1 and TF_2 for the calculation of Z_M.

We used the curve of variation of the modulus E as a function of the temperature of the new HDPE material with 40% birch with a frequency of 20Hz (Fig. 1). This curve was obtained experimentally by the DMA method [11].

We notice that the DMA curve of HDPE40B (40B3 20Hz) has a linear variation in the temperature range from 25°C to 120°C. This curve can be modeled by the straight line passing through the points A (30°C, 4750 MPa) and B (100°C, 1650 MPa) whose equation is:

$E = -44.29T_f+6078.7$ (13) T_f in °C.

Likewise, the static DMA curve of Duracon M90 acetal (Fig. 6) can be modeled by the line passing through the points A(0°C, 3000 MPa) and B(120°C, 550 MPa) whose equation is :
$E = -20.42T_f+3000$ (14) T_f in °C.

Z_M is the material factor; it takes into account the influence of the combination of materials. VDI 2545 Fig. provides the values for the steel-plastic combination; for other combinations we put:

$$Z_M = \sqrt{0.36.E} \quad (15)$$

$$E = \frac{2E_1E_2}{E_1 + E_2} \quad (16)$$

E_1 and E_2 are calculated with the formula (13) or (14).

- **Comparison of the induced contact stress and the allowable stress**

For Duracon M90 acetal material, the initial maximum allowable stress is determined using the curve in Fig. 5. Then for each operating conditions, the allowable stress is calculated by determining the factors K_T, K_V, K_M, K_L and C_s using the tables (tables 3; 4) and the characteristic curves (fig. 3; 4; 6) as for the calculation of the allowable bending stress. Thus the allowable contact stress depends on each operating condition (number of cycles, K_T, K_V, K_M, K_L and C_s).

For the HDPE40B material, still based on the VDI method for determining contact stresses, we know that the induced stress σ_{oc} must be less than or equal to the maximum allowable stress σ_{HN} multiplied by the inverse of the safety factor S_H. We also know that S_H is between $\sqrt{2}$ and 2. In our work we took S_H =1.5. Note that for the material used (HDPE with 40% birch), according to the tensile tests the maximum tensile stress is 38.05 MPa [11]. Normally the curve for the limit stress to contact fatigue must be determined experimentally. For the moment, the fatigue curves for the HDPE40B material have not yet been established. But when the number of operating cycles is less than 1000 cycles, the fatigue limit approaches the tensile limit and the load can be considered static [15]. Thus in our present simulation, for a number of operating cycles less than 1000 cycles we simply compare the stress values obtained at different positions S/pn to the stress value obtained by dividing the maximum tensile stress by the safety factor 1 .5 chosen, or 25.3667 MPa.

- **Verification that each operating point following the normalized positions S/pn is below the C-ω limiting curve; otherwise no operating temperature should be higher than T_{fo}.**

This point is already guaranteed by the condition of establishing the curve C-ω.

We have just finished the complete procedure for the simulation of surface thermal failure. The results from the simulation are presented in the results section.

5. RESULTS AND DISCUSSIONS

In this section, we present the main results and their analyses. Each study case is based on initial specifications.

Case study I: Duracon M90 acetal pinion and gear; Z1 = Z2 = 30 teeth; module m = 2mm; pressure angle α = 20 °; tooth width b = 6.5mm; torque transmitted C = 8.6885Nm; rotation speed ω = 1000rpm.

Case study II: Pinion and gear in HDPE40B composite; Z1 = Z2 = 30 teeth; module m = 2.54mm; pressure angle α = 20 °; tooth width b = 6.5mm; torque transmitted C = 11.5Nm; rotation speed ω = 1000rpm.

5.1 Results for the Duracon M90 Acetal Case Study

To carry out the thermal study, the tooth is meshed (Fig. 7) by a matrix of 6 columns x 12 rows (6x12 nodes), from left to right and from the head towards the center of the tooth. The nodes in column 6, from row 1 to 6, represent the points of the active tooth profile. Table 5 shows the calculated equilibrium temperature at each node for the pinion.

Table 7 shows the evolution of the equilibrium and instantaneous temperatures on the active profiles of the pinion and the gear following the normalized positions on the profile. Thus the greatest instantaneous temperature on the active profile of the pinion is observed at the normalized position S/pn = 0.413 and has a value of TF_1=132.03 °C. That of the gear is observed at the normalized position S/pn = 0.661 and has a value of TF_2=130.90°C.

Similarly, Table 6 shows the equilibrium temperature calculated at each node for the gear.

5.2 Results for the Case Study of the HDPE40B Composite

The tooth mesh is the same as in the case of acetal gears. Table 10 shows the equilibrium temperature calculated at each node for the pinion.

Table 5. Distribution of the equilibrium temperature in the pinion (TB1 in ° C)

		ADDENDUM CIRCLE OF THE TOOTH					
		1	**2**	**3**	**4**	**5**	**6**
TOWARDS	1	28.3861	29.84418	32.8356	36.0397	38.8341	64.1294
ADDENDUM	2	32.1647	37.8014	44.8825	53.0107	61.4221	69.1209
CIRCLE	3	31.4128	38.6120	46.9034	56.0304	65.4433	73.6548
	4	30.7357	38.7461	47.2093	56.4339	66.6426	76.4788
	5	30.4586	39.0767	46.8335	55.2527	65.7037	78.6766
	6	30.7933	40.0979	46.0092	52.3106	60.8156	72.5510
		DEDENDUM CIRCLE OF THE TOOTH					
	7	50.3852	44.2900	45.5206	48.6524	50.4110	44.2641
	8	47.0697	44.2950	44.7281	46.4295	47.1012	44.2635
	9	44.5971	43.4034	43.5528	44.3976	44.6343	43.3662
TOWARDS	10	42.4894	42.0619	42.1183	42.4699	42.5324	42.0189
THE GEAR	11	40.4956	40.5055	40.5307	40.5644	40.5447	40.4564
CENTER	12	38.4465	38.8940	38.8882	38.6040	38.5018	38.8387

Table 6. Distribution of the equilibrium temperature in the gear (TB2 in ° C)

		ADDENDUM CIRCLE OF THE TOOTH					
		1	**2**	**3**	**4**	**5**	**6**
TOWARDS	1	28.4515	30.3503	34.0005	37.9449	41.4144	73.8081
ADDENDUM	2	32.8861	40.4221	49.8586	60.7506	72.1770	82.9249
CIRCLE	3	32.0881	41.4376	52.1908	64.0656	76.4538	87.7362
	4	31.4214	41.6164	52.3376	63.9397	76.7658	89.7067
	5	31.3557	42.1030	51.7777	62.0062	74.2860	89.2986
	6	31.9458	43.5192	50.9152	58.3881	67.8461	80.2569
		DEDENDUM CIRCLE OF THE TOOTH					
	7	56.2426	49.0768	50.6549	54.3579	56.2684	49.0510
	8	52.6650	49.3980	49.9710	51.9800	52.6964	49.3666
	9	50.0693	48.6592	48.8627	49.8595	50.1064	48.6221
TOWARDS	10	47.9036	47.3931	47.4682	47.8827	47.9466	47.3502
THE GEAR	11	45.8779	45.8808	45.9073	45.9469	45.9269	45.8318
CENTER	12	43.7970	44.3135	44.2915	43.9563	43.8523	44.2583

Table 7. Evolution of the equilibrium (TB_1, TB_2) and instantaneous (TF_1, TF_2) temperatures of the pinion and the gear as a function of the normalized position S/pn

S/pn	-1.121	-0.827	-0.744	-0.661	-0.579	-0.496	-0.413	-0.331	-0.248	-0.165	-0.083
TB1	72.55	72.55	72.55	78.68	78.68	78.68	78.68	76.48	76.48	76.48	76.48
TB2	73.81	73.81	82.92	82.92	82.92	82.92	87.74	87.74	87.74	87.74	87.74
TF1	80.22	85.64	93.44	101.02	103.99	106.64	111.31	113.99	116.76	119.37	121.86
TF2	79.19	84.58	94.18	99.73	102.91	105.84	111.10	110.99	112.70	114.32	115.86
S/pn	0.083	0.165	0.248	0.331	0.413	0.496	0.579	0.661	0.744	0.827	1.121
TB1	73.65	73.65	73.65	73.5	73.5	69.12	69.12	69.12	69.12	64.13	64.13
TB2	89.71	89.71	89.71	89.71	89.30	89.30	89.30	89.30	80.26	80.26	80.26
TF1	123.69	125.88	127.99	130.04	**132.03**	129.42	129.59	131.17	128.45	126.83	128.33
TF2	120.72	122.08	123.39	124.66	125.48	126.67	129.54	**130.90**	127.47	126.92	128.16

Similarly, Table 9 shows the equilibrium temperature calculated at each node for the gear.

Fig. 8 shows the evolution of the $SIGMA_C$ induced contact stress following the normalized positions on the pinion tooth profile. This stress is calculated using instantaneous temperatures on the profile.

Fig. 9 shows the C-ω limiting curve for the present case study. The C-ω limiting curve

shows that for any operating point (C, ω) below the limit curve, the profiles of the teeth in contact will not experience surface thermal failure.

Table 10 shows the evolution of the equilibrium and instantaneous temperatures on the active profiles of the pinion and the wheel following the standardized positions on the profile. Thus the greatest instantaneous temperature on the active profile of the pinion is observed at the normalized position S/pn = 0.392 and has a value of TF_1=111.90 °C. That of the wheel is observed at the normalized position S/pn = 0.653 and has a value of TF_2=110.44 °C.

Fig. 10 shows the evolution of the $SIGMA_C$ induced contact stress following the normalized positions on the pinion tooth profile. This stress is calculated using instantaneous temperatures on the profile.

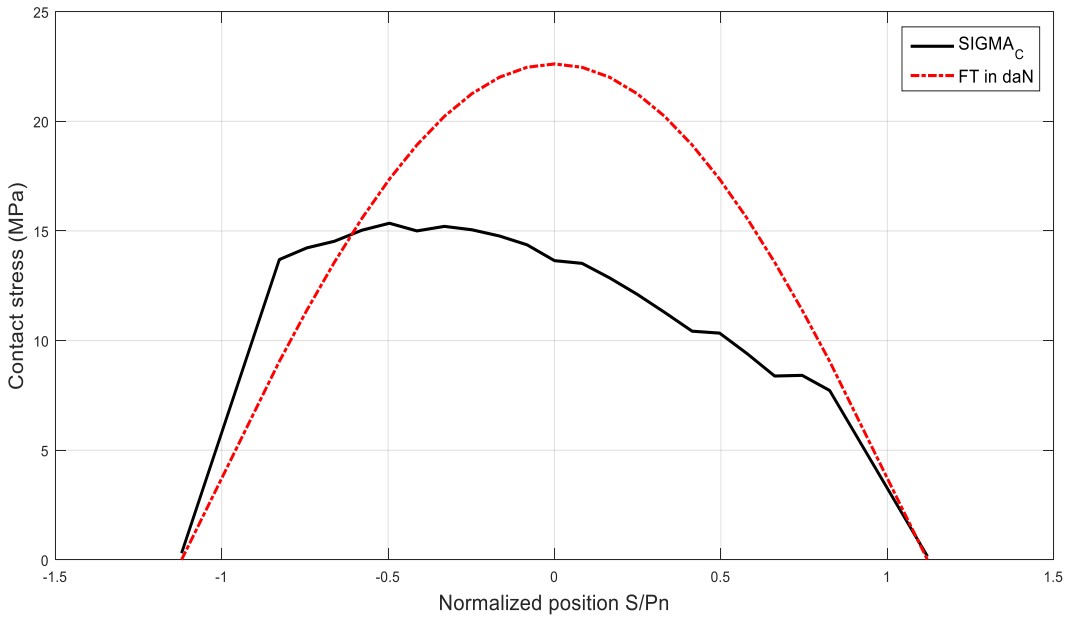

Fig. 8. Evolution of the contact stress on the tooth profile as a function of the normalized position S/pn: Duracon M90 Acetal

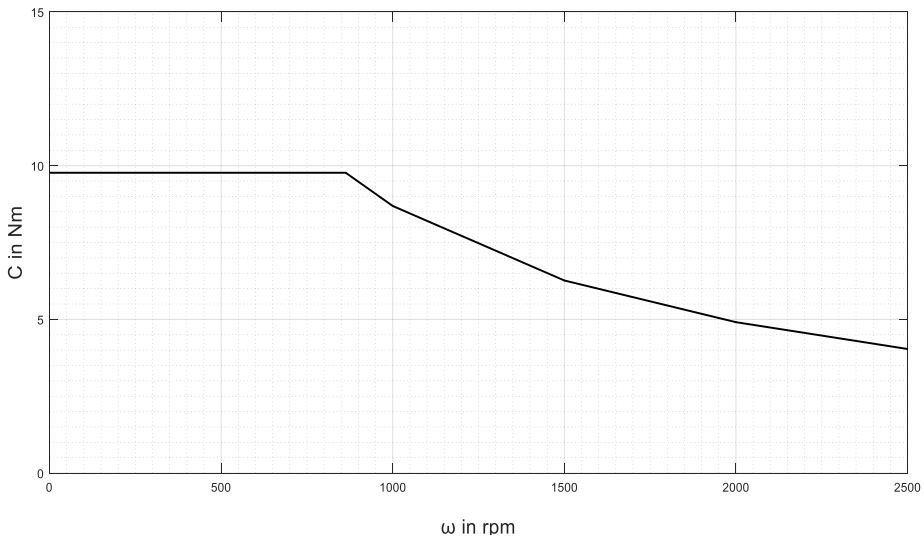

Fig. 9. C-ω limiting curve: Acetal Duracon M90

Table 8. Distribution of the equilibrium temperature in the pinion (TB_1 in ° C)

		ADDENDUM CIRCLE OF THE TOOTH					
		1	**2**	**3**	**4**	**5**	**6**
TOWARDS	**1**	33,9244	35.3450	38.7575	42.4244	45.6806	**57.5297**
ADDENDUM	**2**	37.9067	41.7127	46.6834	52.4611	58.3551	**63.6229**
CIRCLE	**3**	36.7472	41.6910	47.5733	54.2395	61.2901	**67.8556**
	4	35.5395	41.0610	47.1082	53.9423	61.7759	**70.0725**
	5	34.7022	40.5268	46.0689	52.3251	60.3334	**71.1552**
	6	34.5637	40.4346	44.6006	49.2842	55.8103	**65.4416**
		DEDENDUM CIRCLE OF THE TOOTH					
	7	47.1129	42.7410	43.6046	45.8924	47.1421	42.7118
	8	44.2717	42.2860	42.5924	43.8311	44.3058	42.2519
	9	42.0213	41.1738	41.2832	41.8970	42.0605	41.1346
TOWARDS	**10**	40.0184	39.7236	39.7694	40.0245	40.0628	39.6792
THE GEAR	**11**	38.0822	38.1038	38.1290	38.1534	38.1320	38.0540
CENTER	**12**	36.0908	36.4288	36.4336	36.2273	36.1461	36.3735

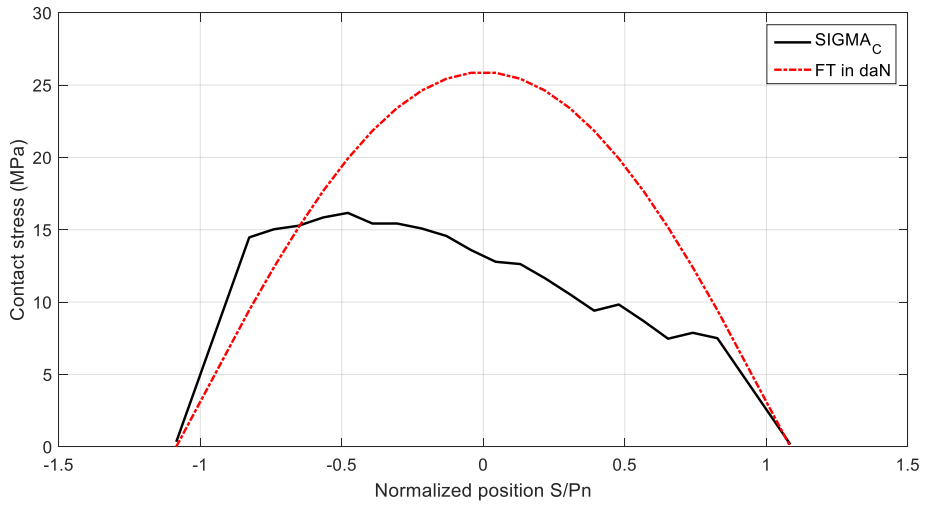

Fig. 10. Curve of the evolution of the contact stress as a function of the normalized position S/pn: HDPE40B

Table 9. Distribution of the equilibrium temperature in the gear (TB_2 in ° C)

		ADDENDUM CIRCLE OF THE TOOTH					
		1	**2**	**3**	**4**	**5**	**6**
TOWARDS	**1**	34.3267	36.2273	40.4556	45.0044	49.0531	**63.7359**
ADDENDUM	**2**	39.0977	44.1462	50.6587	58.2087	65.9633	**73.0213**
CIRCLE	**3**	37.9280	44.3191	51.8364	60.3061	69.2942	**77.8608**
	4	36.7835	43.7989	51.3554	59.7669	69.3339	**79.6797**
	5	36.2557	43.4713	50.2732	57.7345	66.9825	**79.2138**
	6	36.4700	43.7145	48.8287	54.2910	61.4882	**71.6569**
		DEDENDUM CIRCLE OF THE TOOTH					
	7	51.9896	46.9284	47.9998	50.6609	52.0188	46.8993
	8	48.9773	46.6744	47.0634	48.5026	49.0114	46.6403
	9	46.6469	45.6598	45.8007	46.5134	46.6861	45.6207
TOWARDS	**10**	44.6068	44.2584	44.3149	44.6109	44.6511	44.2141
THE GEAR	**11**	42.6506	42.6675	42.6935	42.7217	42.7003	42.6178
CENTER	**12**	40.6391	41.0216	41.0171	40.7776	40.6944	40.9664

Table 10. Evolution of the equilibrium (TB_1, TB_2) and instantaneous (TF_1, TF_2) temperature of the pinion and the gear as a function of the normalized position S/pn

S/pn	-1.085	-0.827	-0.740	-0.653	-0.566	-0.4786	-0.3916	-0.3046	-0.2176	-0.1305	-0.0435
TB1	65.44	65.44	65.44	71.16	71.16	71.16	71.16	70.07	70.07	70.07	70.07
TB2	63.74	63.74	73.02	73.02	73.02	73.02	77.86	77.86	77.86	77.86	79.68
TF1	70.20	74.44	81.39	88.60	90.25	92.30	96.48	99.37	101.53	103.57	105.52
TF2	69.16	73.37	82.19	86.15	89.31	91.61	96.27	96.02	97.36	98.62	101.65
S/pn	0.044	0.131	0.218	0.305	0.392	0.477	0.566	0.653	0.740	0.827	1.085
TB1	70.07	67.86	67.86	67.86	67.86	63.62	63.62	63.62	63.62	57.53	57.53
TB2	79.68	79.68	79.68	79.68	79.21	79.21	79.21	79.21	71.66	71.66	71.66
TF1	107.37	106.93	108.65	110.30	**111.90**	109.21	109.85	111.05	108.24	105.82	107.67
TF2	102.80	103.90	104.96	105.998	106.51	107.47	109.27	**110.44**	108.00	106.58	106.93

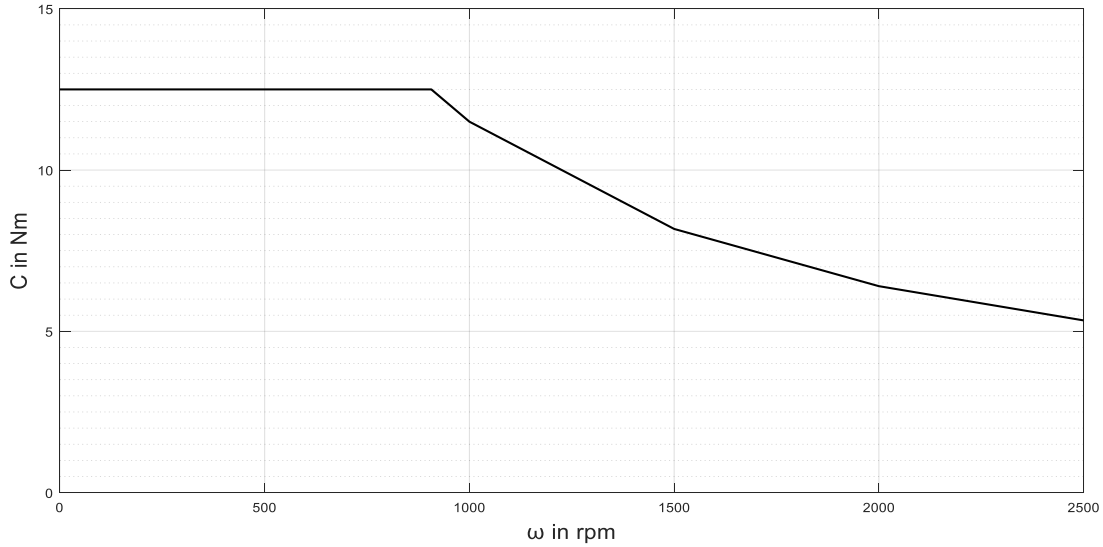

Fig. 11. C-ω limiting curve: HDPE40B

Fig. 11 shows the C-ω limiting curve for the present case study. The C-ω limiting curve shows that for any operating point (C, ω) below the limit curve, the profiles of the teeth in contact will not experience surface thermal failure.

After the presentation of the results, we address in the following section the study of the influence of operating parameters.

5.3 Influence of Torque and Speed on Surface Thermal Failure

Fig. 12 shows the combined influence of torque and speed on surface thermal failure. We note that a more severe operating pair (torque, speed) gives a lower induced operating stress.

Fig. 13 compares the induced stresses and the limiting stresses and shows that, although having lower induced stresses, the more severe operating conditions are those which are less sensitive to surface thermal failure.

5.4. Analysis of Results

First of all, we make a first constant that the results are similar for the two materials studied. The difference in the results lies only at the level of the numerical values, for this reason the comments on the observed thermal failure behavior apply to both materials.

- **Heat map**

Tables 5, 6, 8, and 9 are the equilibrium temperature heat maps. This heat map shows the equilibrium temperature distribution inside the tooth according to the mesh points (fig. 7). It shows that the temperatures are higher on the contact profiles, which is quite normal. For the cases studied, the maximum values are 78.68°C for the acetal driving gear, 71.16°C for the acetal driven gear, 89.71°C for the HDPE40B driving gear and 79.68°C for the HDPE40B driven gear. Tables 7 and 10 show the heat maps of the instantaneous temperature. The instantaneous temperature heat map shows the evolution of the instantaneous temperature on the contact profile following the normalized position. For the cases studied, the maximum values are 132.03°C for the acetal driving gear, 130.90°C for the acetal driven gear, 111.90°C for the HDPE40B driving gear and 110.44°C for the HDPE40B driven gear.

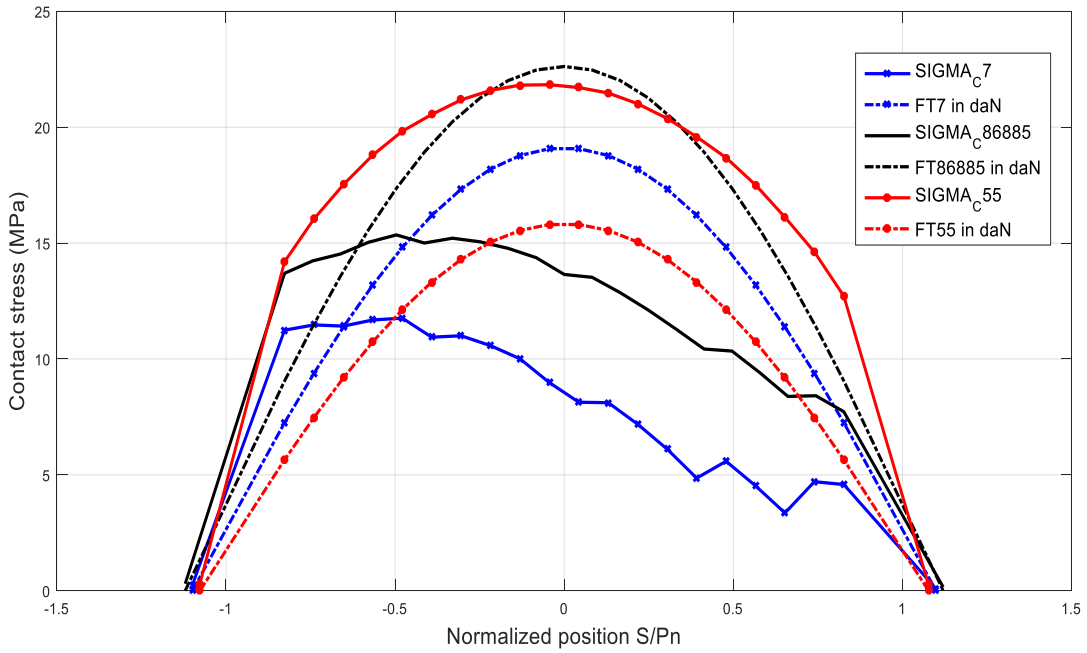

Fig. 12. Influence of torque and speed on the evolution of the contact stress as a function of the normalized position S/pn: Acetal Duracon M90; (7Nm, 1500rpm); (8.6885Nm, 1000rpm); (5.5Nm, 500rpm)

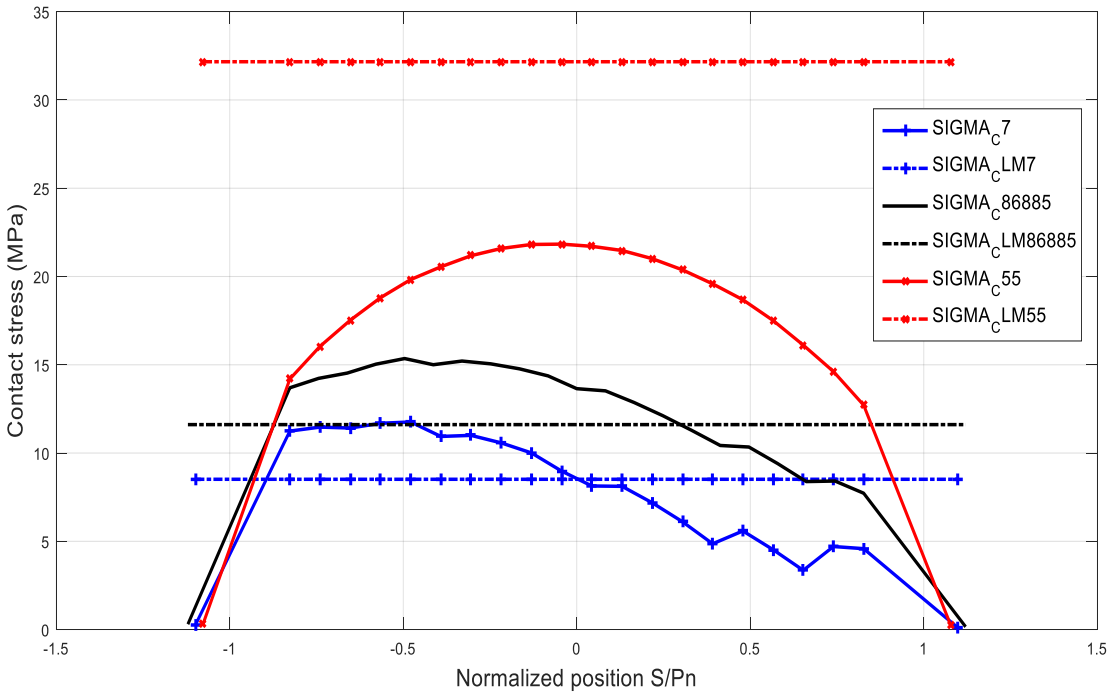

Fig. 13. Comparison of induced contact stress and limit stress for checking thermal failure of different operating points: Acetal Duracon M90; N=10^6 cycles; (7Nm, 1500rpm); (8.6885Nm, 1000rpm); (5.5Nm, 500rpm)

- **Distribution of contact stress as a function of normalized position**

Fig. 8 and 10 show the distribution of contact stress as a function of normalized position. Note that the contact stress is the same at the contact point for the driving gear and the driven gear. For acetal/acetal meshing, the maximum induced stress appears at the normalized position Spn = -0.496 and its value is $SIGMA_C$=15.353 MPa. For the HDPE40B/HDPE40B mesh, the maximum induced stress appears at the normalized position Spn = -0.479 and its value is $SIGMA_C$=16.164 MPa.

- **Influence of torque and speed; comparison of induced stress and allowable stress**

Fig. 12 shows the combined effect of torque and speed on stress and shows us an interesting behavior of it. Indeed we observe that when the operating conditions become more severe (larger torque and/or speed), the maximum stress induced, on the other hand, becomes smaller. The obvious question to ask is, would more severe conditions be more favorable to thermal failure? But the answer is no. First of all we understand this phenomenon by the fact that more severe conditions generate higher temperatures, which in turn reduce the equivalent modulus and this leads to a larger contact surface. If it is the speed alone that has increased, then the force has remained constant and the contact area has increased, then the stress must become smaller. Even when the torque alone has increased, the effect of increasing the surface area outweighs the effect of increasing the force and we still have a smaller stress. Now if we observe the results in fig. 13, we see that the less severe functioning point (5.5Nm, 500rpm) stand the thermal failure, since the allowable fatigue stress $SIGMA_CLM55$= 32.165 MPa is well above the induced stresses of which the maximum value is $SIGMA_CMax55$ = 21.833MPa. On the other hand, the more severe points (8.6885Nm, 1000rpm) and (7Nm, 1500rpm) do not stand the thermal failure, since we have the allowable fatigue stress $SIGMA_CLM86885$ = 11.61 MPa which is below the maximum induced stress $SIGMA_CMax86885$ = 15.353 MPa, as well as the allowable fatigue stress $SIGMA_CLM7$ = 8.514 MPa which is below the maximum induced stress $SIGMA_CMax7$ =

11.76MPa. Note that the values of the limit allowable fatigue stresses are determined for one million (10^6) cycles, using the data in the tables and characteristic curves. An initial value is determined using fig. 5, then adjusted by the factors K_V, K_T, K_L, K_M and C_S which would apply for the determination of the limit allowable bending fatigue stress. For the moment, we do not have data to determine the allowable fatigue stress limits for the HDPE40B composite material. For the operating point studied (11.5Nm, 1000rpm), if the allowable contact fatigue limit stress determined for a given number of cycles with the temperature generated by this operating point exceeds the maximum induced stress $SIGMA_CMAX115$ = 16.164 MPa, this point of operation stand the surface thermal failure.

- **Verification of the C-ω limiting curve**

Fig. 9 and 11 show the C-ω curves for the two cases studied. Normally, any operating point which is located below these C-ω limiting curves must be resistant to thermal failure. But for the case of acetal, the operating point (8.6885Nm, 1000rpm) which is located on the limit curve does not stand the thermal failure, quite simply that the operating temperature T_{fo} of 132°C was defined too high. We must find this operating limit temperature for a given number of cycles, with which any operating point which would generate a temperature less than or equal to this would be resistant to surface thermal failure. We looked it up and found an operating temperature of T_{fo} = 99°C.

6. CONCLUSION

The main results from our work are presented and discussed.

The results showed that the methodological approach implemented in this study can adequately predict surface thermal failure for each given number of cycles. Furthermore, the results showed that the predefined operating temperature T_{fo} ($T_{fo} = \eta T_f$) must be sufficiently lower than the melting temperature T_f of the material, in order to be able to construct the C-ω limiting curve which delimits for a chosen number of operating cycles, the area of operating points which are due to surface thermal failure.

The results also showed that the surface thermal failure behaviors for plastics and composites gears are similar and the higher the melting temperature of the material, the butter it can stand surface thermal failure in more severe working conditions.

COMPETING INTERESTS

Authors have declared that no competing interests exist.

REFERENCES

1. Koffi D, Analysis of methods for sizing plastic gears, Technology watch note produced for CETIM (Senlis) – France; 2004.
2. Kess K, Successful Application of Plastic Gear, 3e CMET, Paris. 1992:721 – 728.
3. Dvorak PJ, More Bite for Plastic Gears, Machine Design. 1988;75 –80.
4. Cathelin J, Modeling of mechanical behavior for gears in reinforced plastic; Doctoral Thesis (Ph.D.), INSA de Lyon; 19 march 2014.
5. Sedjro BK, Modeling of temperature for gears in natural fibers polymers composites. Master Thesis in Mechanical, ENSI, University of Lome, December 2017.
6. Kelley JW, Polymers get in gear, Machine Design. 1997;63 –66.
7. Miel R. Delphi hopes to steer way to growth, Plast. News (USA) 14, No.31, Sept.02; 1–20.
8. Nyametso L, Study of surface thermal failure prediction for gears in natural fibers polymers composites. Master Thesis in Mechanical, ENSI, University of Lome; 2017.
9. Mao K, Li W, Hooke CJ, Walton D, Friction and wear behavior of acetal and nylon gears, ELSEVIER, Wear 267. 2009; 639-645.
10. Kukureka SN, Chen YK, Hooke CJ, Liao P, The wear mechanisms of acetal in unlubricated rolling-sliding contact, ELSEVIER, Wear 185. 1995; 1-8.
11. Wafiuddin et al., Investigation on wear characteristic of biopolymer gear, 4th International Conference on Mechanical Engineering Research (ICMER2017), Materials Science and Engineering 257. 2017;012068 DOI:10.1088/1757-899X/257/1/012068
12. Singh PK, Siddhartha, and Singh AK, An investigation on the thermal and wear behavior of polymer based spur gears. Tribology International, 2018;118:264-272.

13. Herba Y, Metrological characterization study of gear wear of natural fiber-thermoplastic/birch composites and nanocomposites, Master's Thesis, University of Quebec at Trois-Rivières, CANADA; 2022.
14. Koffi D, Bellosta M, Barriol M, Bop C, Surface Thermomechanical Damaging of Plastic Gear Teeth, 15th Canadian congress of applied mechanics, University of Victoria, Victoria, C.-B., Canada; 1995.
15. Mijiyawa F, Formulation, Characterization, Modeling and prediction of the thermo-mechanical behavior of plastic and wood fiber composite parts: Application to Gears, Mechanical Engineering, Doctoral Thesis (Ph.D.), University of Quebec at Trois Rivières;2018.
16. Qtcgears.com Magazines, www.yumpu.com : Section 18 design of plastic gears 18.1 General – Quality; 2011.
17. Koffi D, Study of the Thermal Behavior of Plastic Spur Cylindrical Gears, Doctoral Thesis (Ph.D.) in Mechanical Engineering, Ecole Polytechnique de Montréal; 1987.
18. Drouin G, GOU M, Thiry P, Vinet R, Machine elements, second edition review and increased, Editions of Polytechnic School of Montreal.

Peer-review history:
The peer review history for this paper can be accessed here:
https://www.sdiarticle5.com/review-history/111497